

# Instabilities in an inductively coupled oxygen plasma

C S Corr, P G Steen and W G Graham

School of Mathematics and Physics, Queen's University Belfast, Belfast BT7 1NN, UK

E-mail: c.corr@qub.ac.uk

Received 16 December 2002, in final form 17 March 2003

Published 22 April 2003

Online at [stacks.iop.org/PSST/12/265](http://stacks.iop.org/PSST/12/265)

## Abstract

A reproducible instability, which appears similar to those reported previously, has been observed and studied in a low-pressure 13.56 MHz inductively coupled gaseous electronics conference rf cell operating in oxygen. The instability has been observed in the form of periodic modulations in the light output, floating potential, electron and positive and negative ion densities. The magnitude and frequency of the modulations is sensitive to the plasma operating conditions and the modulation amplitude has been observed to be as high as 40%. The instability is observed in a pressure and power regime where both the capacitive and inductive modes can exist. The frequency of the oscillations increases with increase in gas pressure from 3 to 21 kHz. This pressure window coincides with the pressure regime where there exists a significant fraction of negative ions in both modes. Time-resolved measurements of the electron energy distribution functions and charged particle densities indicate that at all phases of the instability, the plasma parameters remain close to those of the inductive mode. A global model has been modified for an oxygen discharge and this provides a qualitative description of the instability. The global model predicts a smaller power and pressure window for the instability but it can provide a framework for the discussion of instabilities in weakly electronegative discharges.

## 1. Introduction

Low-pressure inductively coupled discharges operating with electronegative gases are increasingly being used for industrial materials processing such as etching and deposition. These high-density discharges have been assumed to be stable, producing relatively quiescent glow discharges. However, recent publications [1–3] have shown instabilities to be present under certain operating conditions. This paper is motivated by these observations. Tuszewski [1], studying O<sub>2</sub> and Ar/SF<sub>6</sub> discharges created in a cylindrical inductively coupled configuration driven at 0.46 MHz observed self-excited modulations in the ion current of a cylindrical Langmuir probe with frequencies in the range 1–40 kHz. More recently, in SF<sub>6</sub> and Ar/SF<sub>6</sub> discharges created using a planar coil configuration driven at 13.56 MHz, Lieberman's group [2, 3] observed a temporal modulation of the optical emission and of the charged particle densities with frequencies in the range 1–900 kHz.

Lieberman's group has developed a global model to describe the instability in SF<sub>6</sub> and Ar/SF<sub>6</sub> mixtures [2, 3]. Since these instabilities have only been observed in electronegative gases, their model focuses on a relaxation oscillation driven by the balance of electrons and negative ions. In capacitive (E) mode, the electron density builds up rapidly reaching a quasi-equilibrium state which allows a transition to the inductive (H) mode. The negative ion density continues to grow relative to the electron density until the H-mode is no longer sustainable whereupon the plasma switches back to the E-mode and the cycle repeats itself. The model examines the dynamic behaviour of the system by solving the electron and negative ion balance equations, together with the energy balance equation. The model yielded results that qualitatively correspond to the experiments. However, the predicted modulation frequencies were lower than those observed and the instability windows in power and pressure were considerably smaller than those seen in the experiment [2, 3].

In order to extend the study of this phenomena we have chosen to work with oxygen discharges because the negative ion fraction ( $\alpha = n_-/n_e$ ) is generally lower ( $\sim 0.2$ ) than in SF<sub>6</sub> containing gas mixtures ( $\sim 100$ ), the negative ion destruction mechanisms are different in oxygen and SF<sub>6</sub> and oxygen is a relatively simple molecular gas with a good database of reaction rates available. On the experimental side we have made time-averaged and time-resolved measurements of the electron energy probability functions (EETFs) and the electron and positive ion densities using Langmuir probes and the negative ion density using a photodetachment technique.

## 2. Experimental apparatus

The present measurements were carried out in a gaseous electronics conference (GEC) reactor (figure 1(a)) driven at 13.56 MHz and operating in an inductively coupled

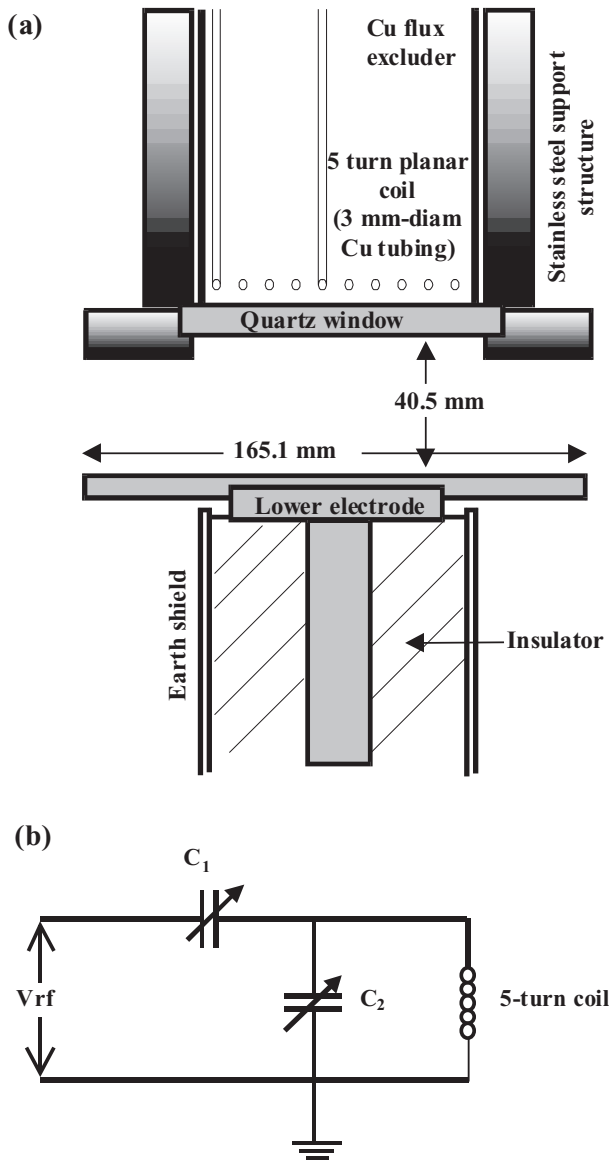


**Figure 1.** Schematic diagram of (a) the inductively coupled GEC reference cell and (b) the rf circuit used to power the coil.

configuration [4] in oxygen. The upper antenna is a planar 5-turn water-cooled copper coil that couples power to the plasma through a quartz window. The lower stainless steel electrode (diameter  $\sim 165$  mm) and the stainless steel vacuum vessels are grounded. The gap between the antenna power coupling window and the bottom stainless steel electrode is  $\sim 40$  mm. The central winding of the upper coil is powered through a close-coupled matching network by an rf power supply, while the outer winding is grounded. The L-type matching network (figure 1(b)) employs two vacuum variable tuning capacitors, with  $C_1 = 5\text{--}55$  pF and  $C_2 = 5\text{--}200$  pF, and is connected directly to the coil to reduce resistive losses. It should be noted that for all measurements reported here the capacitors were adjusted to minimize the reflected power. The input power was recorded as the difference between the forward and reflected power as read from the power supply meter. A turbomolecular pump routinely achieved base pressures of  $10^{-6}$  mTorr before oxygen was flowed through the chamber, and the pumping was throttled to maintain gas pressures in the range 1–100 mTorr determined by a capacitive monometer.

Although described as an inductively coupled system, since the present system has no Faraday shield, it can operate in two modes—a capacitive E-mode at low power and an inductive H-mode at higher power [5]. The transition between the two modes is abrupt but exhibits hysteresis [5]. This mode transition is evidenced by a significant change in the intensity of the light output and in the electron density. The hysteresis phenomenon is illustrated in figure 2. For example, if at a pressure of 50 mTorr, the power is increased, the discharge is ignited in E-mode, characterized by relatively weak light emission. As the power is increased there is a sudden transition to a brighter, H-mode at  $\sim 320$  W. When the power is then decreased a sudden transition back to the E-mode occurs at a lower power of  $\sim 210$  W. The instability discussed later is observed to occur when operating in the apparent H-mode but in a power and pressure regime where both modes can exist (figure 2).

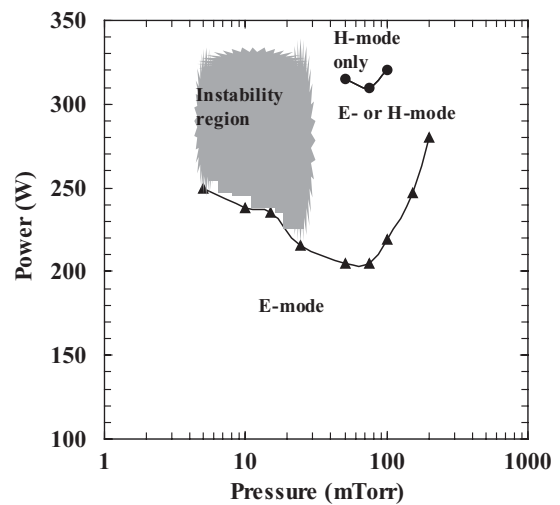


**Figure 2.** The power and pressure at which E- and H-modes are observed in the plasma system, illustrating the hysteresis in the power coupling modes in an oxygen plasma.

For the work reported here, the plasma was characterized at the geometric centre of the inter-electrode gap (2 cm from lower electrode) using several diagnostics. The light emission was collected and transmitted in a quartz optical fibre to a fast photodiode with spectral response from 450 to 1064 nm. An unbiased Langmuir probe provided measurements of the floating potential. A passively compensated Langmuir probe [6] was used to find the plasma parameters from measurements of the probe  $I(V)$  characteristics using a Smartsoft data acquisition system. The EEPFs were determined from the second derivative of the  $I(V)$  characteristics [7]. The electron and ion densities were calculated from the respective saturation currents as determined from the  $I(V)$  curve [8]. The compensated Langmuir probe design was similar to that reported previously [9]. It was made from a 0.125 mm diameter nichrome wire with 17 mm extended beyond the surrounding alumina insulator to form the probe tip. The compensated probe system consisted of the measurement probe and a separate floating reference probe to correct for fluctuations in the direct current value of the plasma potential. The probes were cleaned at regular intervals in argon discharges by drawing electron currents sufficient to have the tip glow bright red. A set of benchmark time-averaged plasma parameters at specific plasma operating conditions were used to determine reproducibility and to check for any longer term drifts in the plasma or measurement techniques.

A probe-based laser photodetachment technique was used to measure the negative ion density [10, 11]. This experimental arrangement consisted of a 5 mm diameter cylindrical beam, from a frequency doubled Nd:YAG laser (532 nm), aligned to be collinear with an uncompensated 0.5 mm diameter, nichrome wire probe positively biased to detect electrons detached from the negative ions. The necessary conditions [10, 11] for probe voltage and laser beam power conditions were determined to insure that the negative ion fractions were measured correctly. The laser photon energy (2.3 eV) was sufficient to photodetach  $O^-$ ,  $O_2^-$  and  $O_3^-$  ions which have electron affinities of 1.46 eV, 0.44 eV and 2.1 eV, respectively [12, 13]. The negative ion density was determined from measurements of the electron saturation current ( $I_{dc}^-$ ) in absence of the laser pulse and the increase in the current ( $\Delta I^-$ ) immediately after the pulse using the relationship [10, 11]

$$\frac{\Delta I^-}{I_{dc}^-} = \frac{\Delta n_e}{n_e} = \frac{n_-}{n_e}$$

where  $n_e$  and  $n_-$  are the electron and negative ion densities, respectively. The measured dependence of the photodetachment signal on laser beam energy confirmed that the dominant negative ion in the present discharge is  $O^-$  [10, 11].

Time-resolved probe-based photodetachment measurements were determined at 10  $\mu s$  intervals by triggering on a pulse obtained at a specific phase of the instability observed on the output of the photodiode. A delay generator between this pulse and the trigger input of the laser allowed measurements to be made at regular intervals throughout the instability. Time-resolved measurements of the electron and positive-ion saturation currents were made by biasing the Langmuir probe at +50 V and -40 V, respectively. The time-resolved electron and positive ion densities were obtained by calibrating these

measurements against the measured time-averaged electron and positive ion densities.

The Smartsoft data acquisition system and a compensated Langmuir probe were used to determine time-resolved probe  $I(V)$  characteristics. A trigger pulse was obtained from the optical emission and a delay was set at 10  $\mu s$  intervals. The data acquisition system was programmed to measure the probe current at one probe voltage, with a 30  $\mu s$  resolution, after the trigger pulse. Following subsequent trigger pulses, the current was measured either at the same probe voltage or a different probe voltage, allowing both averaging and the build up of an entire  $I(V)$  characteristic. The total acquisition time was  $\sim 3$  min. The  $I(V)$  characteristics were then numerically differentiated to obtain the second derivative and hence the time-resolved EEPFs.

### 3. Experimental results

#### 3.1. The instability

The instability was routinely observed in the form of periodic oscillations in the outputs of both a photodiode and an unbiased Langmuir probe at the centre of the system (figure 3) when operating with oxygen. The period and fractional changes are the same for both the measurements. It can be seen that the frequency of the instability at 11 mTorr and 238 W is about 10 kHz. The instability is dependent on the axial probe position (figure 4). The amplitude decreases with distance from the quartz window. For the probe positions shown a peak modulation of about 40% is observed at 3 cm above the lower electrode. Both the frequency and magnitude of the instability are sensitive to gas pressure (figure 5). The instability is observed for input powers from  $\sim 230$  to 340 W and gas pressures from 5 to 23 mTorr but only when the discharge is in H-mode (figure 2). Over this range of conditions the frequency of oscillation scales with pressure ( $p$ ) as a power law of approximately  $p^{1.5}$ . The frequency increases from 3 to 21 kHz as the gas pressure changes from 5 to 23 mTorr; the frequency does not vary significantly with power. Figure 5(b) shows how the instability grows to a maximum at a pressure of  $\sim 11$  mTorr and then decreases until it disappears at  $\sim 23$  mTorr.

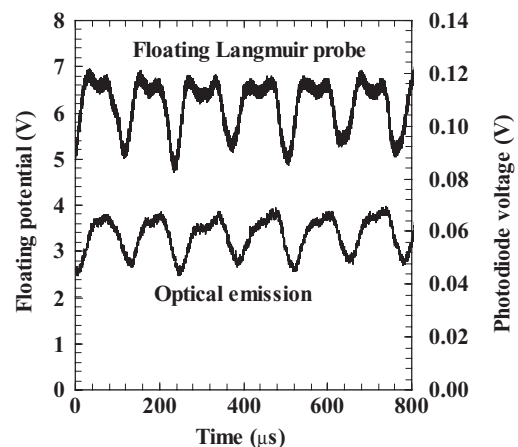


**Figure 3.** The time variation of the floating Langmuir probe current and the optical emission from an oxygen discharge at 11 mTorr and 238 W.

The amplitude of the instability also varies with input power (figure 6). Below  $\sim 240$  W there is a distinct transition to a quiescent E-mode. As the input power is increased, the amplitude of the instability decreases. This suggests that

the discharge may be entering a quiescent inductive mode. However, the range of the rf power supply did not permit for this to be investigated further. Instabilities were not observed when operating in an argon discharge.

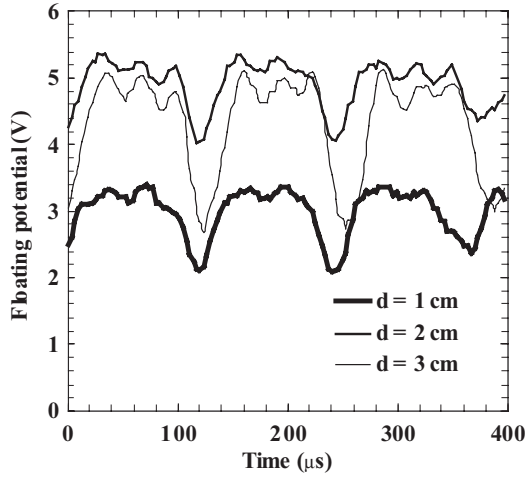


**Figure 4.** The spatial dependence of the floating Langmuir probe current with distance from grounded electrode ( $d = 0$ ).

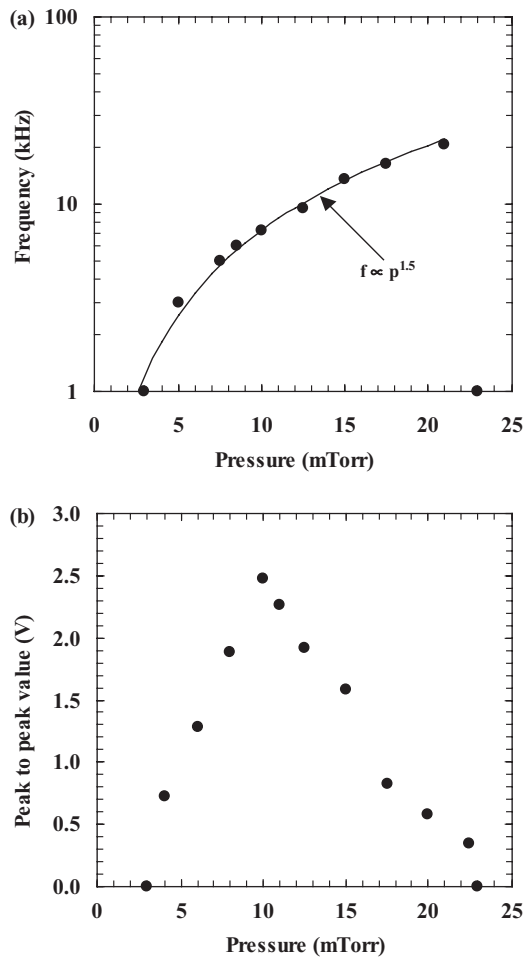


**Figure 5.** (a) The pressure ( $p$ ) dependence of (a) the frequency of the instability ( $\bullet$ ) with a curve proportional to  $p^{1.5}$  and (b) of the peak-to-peak amplitude at 239 W.

### 3.2. Time-averaged measurements

There are significant differences in the plasma parameters for the capacitive and inductive modes. As illustrated in figure 7 the measured EEPF in the inductive mode can be best described as a Maxwellian depleted at the higher energies whilst in the capacitive mode it is bi-Maxwellian. The electron density in the inductive mode is much higher than that in capacitive mode. For example, under the power and

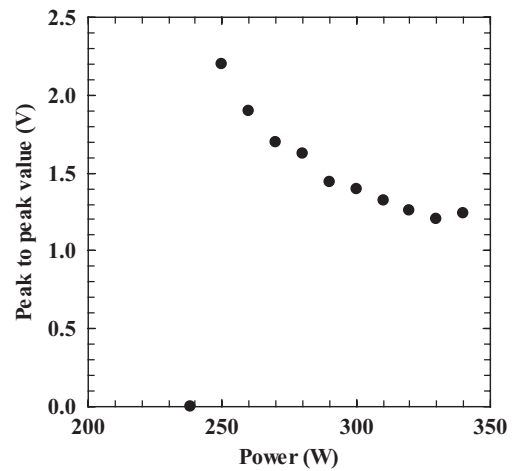


**Figure 6.** The dependence of the peak-to-peak amplitude of the instability on the measured forward power.

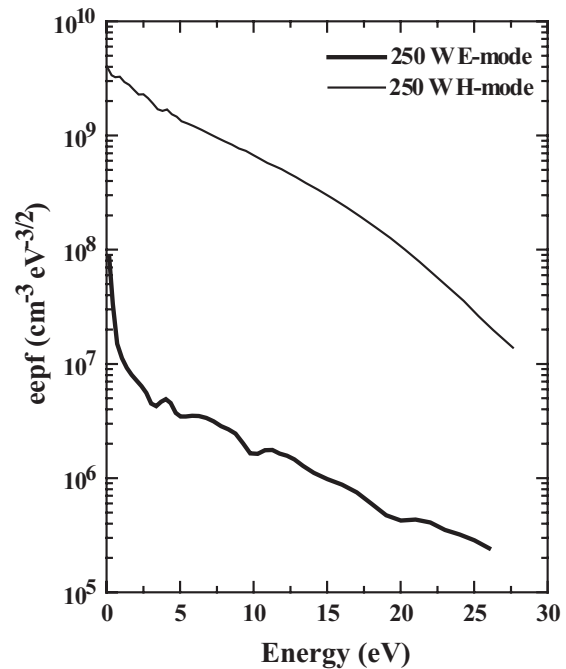


**Figure 7.** The time-averaged EEPFs in the H- and E-modes at 250 W operating at a gas pressure of 10 mTorr.

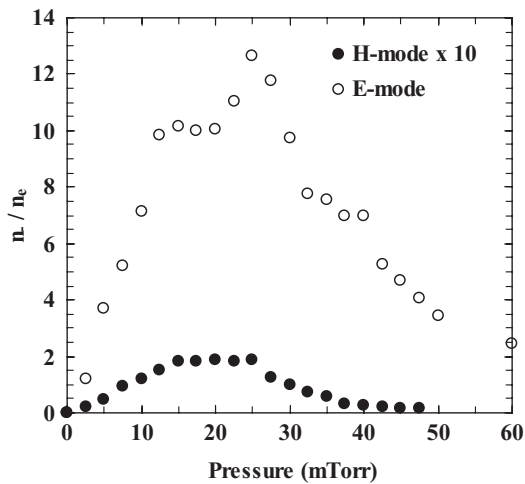


**Figure 8.** The time-averaged negative ion fractions as a function of pressure in capacitive (O) and inductive modes (● × 10) at 275 W.

pressure conditions where the instability has its maximum amplitude (11 mTorr and 250 W), the electron density in the inductive mode is  $\sim 5 \times 10^{10} \text{ cm}^{-3}$  with electron temperatures of  $\sim 5 \text{ eV}$ . The capacitive mode consists of a low energy electron population of density  $\sim 4 \times 10^7 \text{ cm}^{-3}$  and a higher energy electron population of density  $\sim 9 \times 10^7 \text{ cm}^{-3}$  with electron temperatures of  $\sim 1 \text{ eV}$  and  $\sim 8.5 \text{ eV}$ , respectively.

The time-averaged negative ion density is greater in the inductive mode ( $\sim 6 \times 10^9 \text{ cm}^{-3}$ ) than in the capacitive mode ( $\sim 2 \times 10^9 \text{ cm}^{-3}$ ). However, the negative ion fraction,  $\alpha$ , is  $\sim 7$  in the capacitive mode and  $\sim 0.1$  in the inductive mode at these conditions. This is due to the much higher electron density in the inductive mode. In fact, under all conditions measured, the capacitive mode is much more electronegative than the inductive mode (figure 8). It should be noted that the instability is only observed in a pressure regime where there is a significant negative ion fraction.

### 3.3. Time-resolved measurements

In the centre of the discharge i.e. 2 cm from the grounded electrode, time-resolved Langmuir probe and photodetachment measurements were made at intervals through the time period of the instability. From figure 9 it can be seen that the negative ion fraction varies through the instability in the same way as the optical and floating probe signal measurements. With increasing pressure, the frequency of the oscillation of the negative ion fraction increases. The peak-to-peak amplitude of the change in the negative ion fraction also increases with increasing pressure to a maximum at approximately 11 mTorr and then decays until it disappears. These results are consistent with figure 5. In figure 10 time-resolved measurements of the electron, positive ion and negative ion densities taken at 11 mTorr and 275 W are shown along with time-resolved negative ion fractions. When the electron and positive ion densities are at a maximum the negative ion density and fraction are at a minimum. It can be seen that the measured electron density oscillates between  $\sim 6 \times 10^{10}$  and  $\sim 5.5 \times 10^{10} \text{ cm}^{-3}$ . Over the same time period, the measured positive ion density

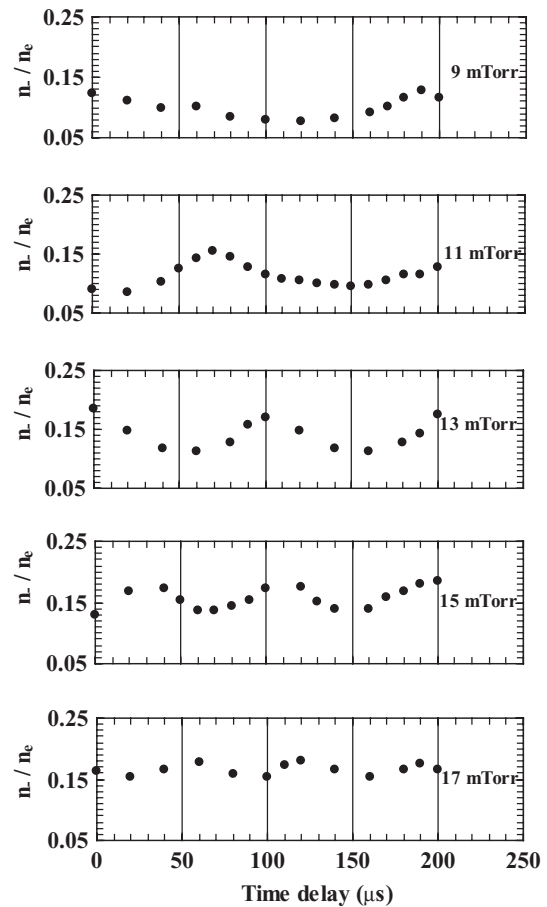


**Figure 9.** The time variation of negative ion fraction as a function pressure at 275 W.

varies between  $\sim 9.2 \times 10^{10}$  and  $\sim 8.2 \times 10^{10} \text{ cm}^{-3}$  and the measured negative ion density oscillates between  $\sim 9 \times 10^9$  and  $\sim 5 \times 10^9 \text{ cm}^{-3}$ . These density values are typical of time-averaged values measured in the inductive mode. The time-resolved EEPF measurements showed the same depleted Maxwellian distribution as that measured in the time-averaged inductive mode.

## 4. Global model of instability

A volume-averaged global model for the instability was initially developed by Lieberman *et al* [2] and has been subsequently refined in Chabert *et al* [3]. The input parameters are the input power and gas density, the system geometry, details of the electrical circuit and the appropriate rate coefficients. As discussed below, the model calculates dynamic behaviour of the particle densities and the electron temperature.

We have modified this model for use with an oxygen discharge operating in a GEC inductive reactor. The most important modifications are in using the kinetics of oxygen rather than SF<sub>6</sub> and Ar/SF<sub>6</sub> discharges and the different geometries. Their system [3] has a surface-to-volume ratio ( $S/V$ ) of  $\sim 25$ , whereas here it is  $\sim 74$  and in the electrical circuits as discussed below.

The particle balance equations for the global model but reflecting an oxygen plasma can be written as

$$\frac{dn_e}{dt} = n_e n_g K_{iz} + n_- n_o K_{o-det} - n_e n_g K_{att} - \Gamma_e \frac{S}{V} \quad (1)$$

$$\frac{dn_-}{dt} = n_e n_g K_{att} - n_- n_o K_{o-det} - n_- n_+ K_{rec} - \Gamma_- \frac{S}{V} \quad (2)$$

where  $V = \pi r^2 l$  and  $S = 2\pi r(r + l)$  are the volume and surface area of the plasma, respectively,  $n_e$ ,  $n_+$  and  $n_-$  are the electron, positive ion and negative ion densities, respectively,  $n_g$  is the total gas density,  $n_o$  is the atomic oxygen density,  $K_{iz}$  is the ionization rate constant,  $K_{o-det}$  is the atomic neutral detachment rate constant,  $K_{att}$  is the dissociative attachment rate constant,  $K_{rec}$  is the positive–negative ion recombination rate constant, and  $\Gamma_e$  and  $\Gamma_-$  are the electron and negative ion flux's to the wall, respectively. The electron and negative ion fluxes to the wall are functions of the plasma potential  $\Phi$  through the Boltzmann relations:

$$\Gamma_e = \frac{1}{4} n_e \bar{v}_e e^{-\Phi/T_e} \quad (3)$$

$$\Gamma_- = \frac{1}{4} n_- \bar{v}_- e^{-\Phi/T_-} \quad (4)$$

where

$$\bar{v}_e = \sqrt{\frac{8kT_e}{\pi m_e}} \quad (5)$$

$$\bar{v}_- = \sqrt{\frac{8kT_-}{\pi m_-}} \quad (6)$$

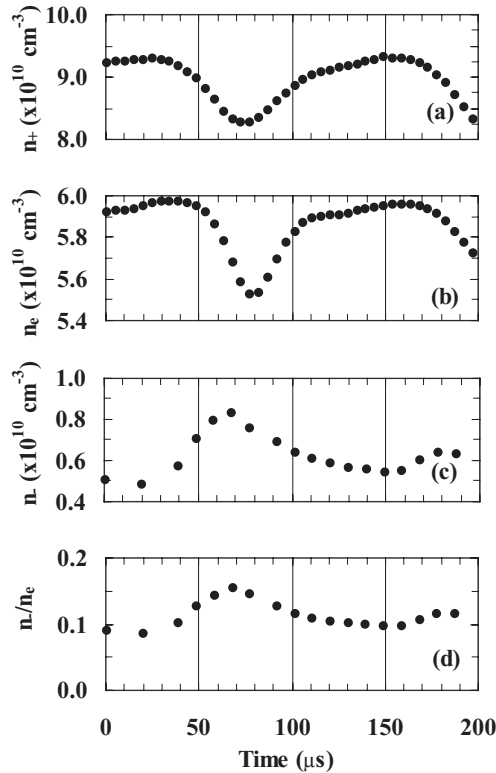


**Figure 10.** The time variation of charge particle densities for (a) positive ions, (b) electrons, (c) negative ion density and (d) the negative ion fraction at 11 mTorr and 275 W.

are the electron and negative ion mean speeds, respectively, where  $T_e$  is the electron temperature,  $T_-$  is the negative ion temperature,  $m_e$  is the electron mass,  $m_-$  is the negative ion mass and  $k$  is Boltzmann's constant. We make the common assumption that the negative and positive ion temperature are the same and a few tenths of an electronvolt, in which case the plasma potential is large that the negative ion flux to the wall can be ignored.

In order to access the important negative ion production and loss mechanisms in the oxygen discharge we have developed a zero-dimensional kinetic code, based on that described in [14]. The reactions that were considered are given in table 1 [14, 15]. With only the gas pressure and the input power as inputs the zero-dimensional model accurately predicted the magnitude of electron density ( $\sim 5.6 \times 10^{10} \text{ cm}^{-3}$  at 10 mTorr) but a lower electron temperature of  $\sim 2.6 \text{ eV}$ . The calculated negative ion densities are a factor of  $\sim 2$  higher ( $\sim 1.6 \times 10^{10} \text{ cm}^{-3}$ ) and the positive ion densities slightly lower than that are found experimentally. The calculated atomic fraction values were close to those measured in experiment [16]. This model predicts a relatively low electronegativity ( $< 0.5$ ) with a similar pressure dependence of the negative ion fraction as that observed experimentally, i.e. having a maximum over the range 7–28 mTorr. From this model we determined that the dominant negative ion loss mechanisms are ion–ion recombination and neutral atom detachment.

Returning to the global model, the kinetics here differ from Chabert *et al* [3] for Ar/SF<sub>6</sub> and SF<sub>6</sub> in that the atomic species plays a significant role so changing the pressure dependencies predicted by the model. The important reaction rates used in equations (1) and (2) are also contained in table 1. The atomic oxygen density has previously been measured and modelled for our system [16]. Here, we use a value of  $2 \times 10^{13} \text{ cm}^{-3}$  as this is the value obtained experimentally when operating in the inductive mode at 10 mTorr and 275 W. Over the present pressure range ( $< 25 \text{ mTorr}$ ) this density can be considered to be constant.

The analysis for the global model follows exactly that of Chabert *et al* [3]. The electron power absorbed,  $P_{abs}$ , is modelled by considering both capacitive and inductive coupling. The voltage powering the coil is supplied by a 50 Ω rf power source through a capacitive matching network (figure 1(b)), where  $C_1$  and  $C_2$  are variable series and parallel capacitors, respectively. For our calculation of the capacitive energy deposition in the discharge due to electron heating we use the electron density of  $1 \times 10^8 \text{ cm}^{-3}$  which we have

**Table 1.** The reaction set for oxygen.

Reaction	Rate coefficient ( $\text{cm}^3 \text{ s}^{-1}$ )
$e^- + \text{O}_2 \rightarrow \text{O}^- + \text{O}$	$K_{att} = 8.8 \times 10^{-11} \exp(-4.4/T_e)$
$e^- + \text{O}_2 \rightarrow \text{O}_2^+ + 2e^-$	$K_{iz} = 2.13 \times 10^{-8} \exp(-14.5/T_e)$
$\text{O}^- + \text{O}_2^+ \rightarrow \text{O} + \text{O}_2$	$K_{rec} = 1.4 \times 10^{-7}$
$\text{O} + \text{O}^- \rightarrow \text{O}_2 + e^-$	$K_{o-det} = 3 \times 10^{-10} (300/T_g)^{1/2}$
$e^- + \text{O}^- \rightarrow \text{O} + 2e^-$	$K_{e-det} = 2 \times 10^{-7} \exp(-5.5/T_e)$
$e^- + \text{O}_2 \rightarrow 2\text{O} + e^-$	$K_{diss} = 4.2 \times 10^{-9} \exp(-5.6/T_e)$
$e^- + \text{O}_2^+ \rightarrow 2\text{O}$	$K_{rec2} = 5.2 \times 10^{-9}/T_e$
$\text{O}^- + \text{O}_2(a^1 \Delta_g) \rightarrow \text{O}_3 + e^-$	$K_{m-det} = 3 \times 10^{-10}$
$\text{O}^- + \text{O}_2^+ \rightarrow 3\text{O}$	$K_{rec3} = 1 \times 10^{-7}$
$e^- + \text{O}_2 \rightarrow e^- + \text{O}_2^*$	$K_{ex} = 2.13 \times 10^{-8} \exp(-10/T_e)$

measured in capacitive mode experimentally. Using values for the radius and length of the coil and the quartz window thickness for our system, we calculate the coil-to-plasma quartz window capacitance to be 60 pF [17]. Again, using our experimental parameters we calculate a sheath width of  $\sim 2$  mm which results in a sheath capacitance of 53 pF. The inductive coupling is modelled using our coil inductance of  $1.2 \mu\text{H}$  and resistance  $0.09 \Omega$  but using the same measured value of  $2 \Omega$  for the plasma resistance as Chabert *et al* [3] which they obtain from Gudmundsson and Lieberman [18].

When implementing this model the matching network capacitors are set so that the system is tuned to the experimentally measured time-averaged value of  $n_e$  ( $5 \times 10^{10} \text{ cm}^{-3}$ ) at 275 W and 10 mTorr which are parameters where the instability is observed experimentally. When varying the pressure in the model the electron density is kept constant since this is approximately true experimentally. For our values of input power (275 W) at a gas pressure of 10 mTorr and the measured electron density, the model finds no unstable behaviour. However, if the input power is reduced instabilities are observed (figure 11). When increasing the pressure it is necessary to decrease the power further for the instability to be maintained. The model then predicts instabilities over a pressure range 6–14 mTorr. The experimental instability is observed from 5 to 23 mTorr. Referring to figure 11, although we input an electron density of  $5 \times 10^{10} \text{ cm}^{-3}$  the model computes a lower electron density which oscillates between  $\sim 1.3 \times 10^{10}$  and a  $\sim 2 \times 10^9 \text{ cm}^{-3}$ . The model also predicts a larger negative ion fraction compared to that measured experimentally.

Unlike the experimental results the model predicts no significant frequency dependence on the gas pressure

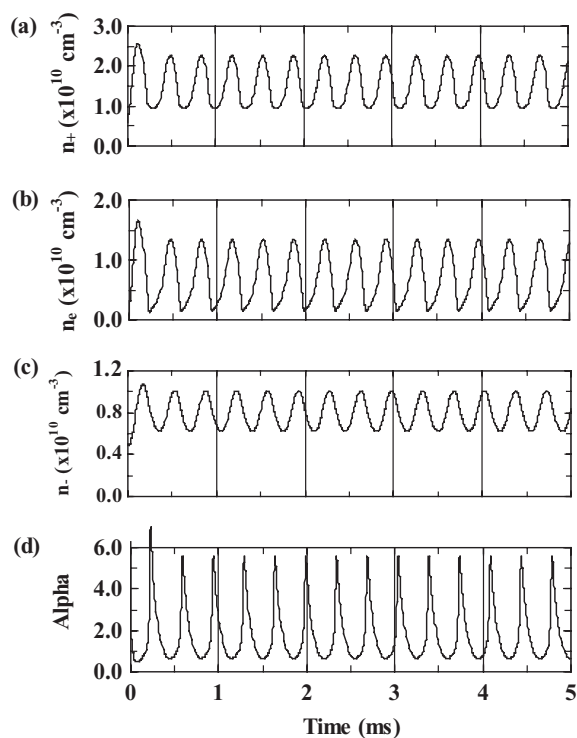


**Figure 11.** The time varying (a) positive ion density, (b) electron density, (c) negative ion density, and (d) negative ion fraction calculated by the global model [3] at 10 mTorr and 103 W.

(figure 12(a)). However, the model does predict a maximum in the amplitude of the modulations at around 10 mTorr (figure 12(b)), which is in agreement with experiment. As in the experimental observations (figure 8) the time-averaged negative ion fraction calculated by the model over this unstable regime displays a maximum (figure 13).

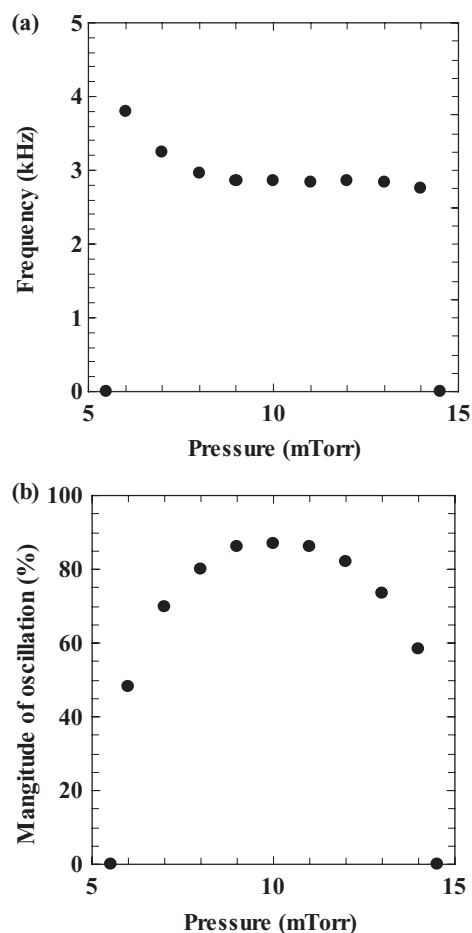


**Figure 12.** The pressure dependence of (a) the frequency and (b) the magnitude of the oscillations as calculated by the global model [3].

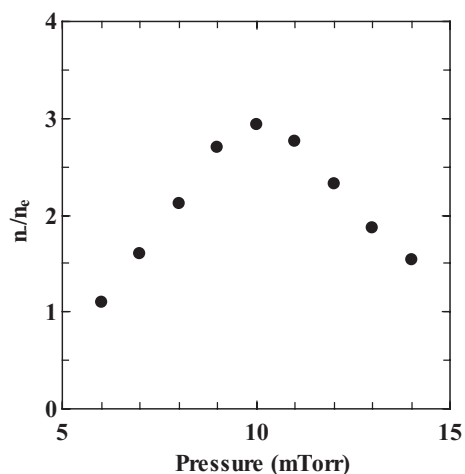


**Figure 13.** The time-averaged negative ion fraction calculated by the global model [3].

## 5. Discussion and conclusion

Instability, in the form of the temporal modulation of light emission, floating potential and electron, positive ion and negative ion densities, has been observed in low-pressure inductively coupled oxygen plasma. The instability is found in inductive mode but in a power and pressure regime where, due to the hysteresis in the capacitive to inductive mode transition, both capacitive and inductive modes can exist. In oxygen discharges, the negative ion fraction is particularly sensitive to the gas pressure and the instability is only found in a pressure region where there is a significant negative ion fraction in both modes.

Time-resolved measurements show that the modulation of the electron and ion densities, the light emission and the floating potential are correlated, while the negative ion density variation is anti-correlated with the above, i.e. the negative ion density drops when they increase in magnitude.

As expected, there are differences between our experimental observations to those of Chabert *et al* [3] for SF<sub>6</sub>. They report a greater range of frequencies (1–100 kHz) and modulation (up to 100%) compared to the present results in oxygen with a frequency range 3–23 kHz and modulation with a maximum of 40%. However, there are some similarities, for example the increase in the frequency of the instability with pressure is observed in both cases however the scaling of the frequency with pressure is different (here we observe a scaling proportional to  $p^{1.5}$  whereas Chabert *et al* [3] report a scaling proportional to  $p^{0.5}$ ).

The model proposed by Chabert *et al* [3] and modified here provides a framework in which to discuss the present experimental results. As in SF<sub>6</sub> the major production mechanism for negative ions in oxygen is through electron attachment to the molecules. While in SF<sub>6</sub> the dominant negative ion loss process is considered to be positive–negative ion recombination and to some degree detachment by metastable molecules. In oxygen our zero-dimensional kinetic model of the oxygen discharge indicated two main destruction mechanisms: detachment by oxygen atoms and ion–ion recombination, in the operating regime where instabilities are observed. This model accurately predicted measured electron density and negative ion fractions and showed the negative ion fraction had a maximum value at 10 mTorr.

Using these reactions in Chabert *et al*'s [3] model we find an instability to occur over a narrow pressure range of 6–14 mTorr, in qualitative agreement with the experiments. Again in agreement with experiment the model predicts the instability to occur over a pressure range where the calculated time-averaged negative ion fraction is largest. The magnitude of the instability varies with pressure as observed experimentally. A significant difference is that the model predicts a smaller instability window for input power and gas pressure compared with experiment and there is no pressure dependence of the instability frequency. This first model of the instability phenomena is a global one and so far from complete. For

example, agreement between the model and the experimental results might be improved if the spatial variation in the densities of the different plasma constituents were included. However, the present results indicate that the global model [2, 3] provides a framework for discussing instabilities in weakly, as well as strongly, electronegative discharges but requires further refinement before quantitative predictions can be made.

In practical terms, these instabilities might present both problems and opportunities. On the one hand, the instabilities may give rise to erratic behaviour in the plasma properties and even motion of the plasma, with consequences for processing performance. On the other, it may be possible to exploit them to create a plasma environment similar to those produced by actively pulsing plasmas.

## Acknowledgments

The authors wish to thank Pascal Chabert and Michael Lieberman for the stimulating conversations on these instabilities and particularly in providing a copy of their global model programme. We gratefully acknowledge the general assistance of Sergi Gomez and Charlie Mahony and to Fernando Garcia for assistance in creating the zero-dimensional kinetic model programme.

## References

- [1] Tuszewski M 1996 *J. Appl. Phys.* **79** 8967
- [2] Lieberman M A, Lichtenberg A J and Marakhtanov A M 1999 *Appl. Phys. Lett.* **75** 3617
- [3] Chabert P, Lichtenberg A J, Lieberman M A and Marakhtanov A M 2001 *Plasma Sources Sci. Technol.* **10** 478
- [4] Graham W G, Mahony C M O and Steen P G 2000 *Vacuum* **56** 3
- [5] Turner M M and Lieberman M A 1999 *Plasma Sources Sci. Technol.* **8** 313
- [6] Cantin A and Gagné R R J 1977 *Appl. Phys. Lett.* **30** 316
- [7] Druyvesteyn M J 1930 *Z. Phys.* **64** 781
- [8] Hopkins M B and Graham W G 1986 *Rev. Sci. Instrum.* **57** 2210
- [9] Mahony C M O, McFarland J, Steen P G and Graham W G 1999 *Appl. Phys. Lett.* **75** 331
- [10] Bacal M, Hamilton G W, Bruneteau A M and Doucet J 1979 *Rev. Sci. Instrum.* **50** 719
- [11] Bacal M and Hamilton G W 1979 *Phys. Rev. Lett.* **42** 1538
- [12] Neumark D M, Lykke K R, Andersen T and Lineberger W C 1985 *Phys. Rev. A* **32** 1890
- [13] Drzaic P S, Marks J and Brauman J I 1984 *Gas Phase Ion Chemistry* vol 3, ed M T Bowers (Orlando, FL: Academic) **3** 167
- [14] Lieberman M A and Lichtenberg A J 1994 *Principles of Plasma Discharges and Materials Processing* (New York: Wiley)
- [15] Gudmundsson J T, Kouznetsov I G, Patel K K and Lieberman M A 2001 *J. Phys. D: Appl. Phys.* **34** 1100
- [16] Gomez S, Corr C S, Steen P G and Graham W G in progress
- [17] Gudmundsson J T and Lieberman M A 1998 *Plasma Sources Sci. Technol.* **7** 83
- [18] Gudmundsson J T and Lieberman M A 1998 *Plasma Sources Sci. Technol.* **7** 1